The Astrophysical Journal, 981:175 (10pp), 2025 March 10 https://doi.org/10.3847/1538-4357/adb618

New Potential Ultracompact X-Ray Binaries for Space-based Gravitational-wave Detectors from a Low-mass Main-sequence Companion Channel

Minghua Chen[1,2] and Jinzhong Liu[1,2]
[1] Xinjiang Astronomical Observatory, Chinese Academy of Sciences, Urumqi 830011, People's Republic of China; liujinzh@xao.ac.cn
[2] University of Chinese Academy of Sciences, Beijing 100049, People's Republic of China
Received 2024 December 12; revised 2025 February 10; accepted 2025 February 12; published 2025 March 7

Abstract

We investigate the formation and evolution of ultracompact X-ray binaries (UCXBs) using the COMPAS binary evolution code, starting from the zero-age main sequence (MS). Focusing on the low-mass MS companion channel, we simulate gravitational-wave (GW) signals from UCXBs with LEGWORK and evaluate their detectability by space-based observatories such as Taiji and TianQin. By incorporating signal-to-noise ratio (SNR) calculations with a threshold of SNR > 5, we provide a realistic framework to assess the detectability of the GW source. Our analysis suggests that the Milky Way currently hosts 7–32 observable UCXBs from the MS companion channel. Taiji or LISA alone could detect one to six sources over an 8 yr observation period, while TianQin, due to its high-frequency sensitivity, contributes to detecting systems with extremely short orbital periods and can also detect one to four sources. Comparison with sensitivity curves validates UCXBs as detectable GW sources, particularly at greater Galactic distances. This study improves our understanding of the evolution of UCXBs and their role as GW sources. By integrating population synthesis, SNR-based analyses, and observational data, we establish UCXBs as significant targets for GW astronomy, paving the way for future missions and theoretical studies of compact binary systems.

Unified Astronomy Thesaurus concepts: X-ray binary stars (1811); Gravitational waves (678); Compact binary stars (283); Space telescopes (1547)

1. Introduction

Ultracompact X-ray binaries (UCXBs) are low-mass X-ray binaries (LMXBs) with ultrashort orbital periods typically less than 60 minutes, consisting of a neutron star (NS) or black hole (BH) accretor and a hydrogen-poor donor star (S. Rappaport et al. 1982; L. A. Nelson et al. 1986). UCXBs play a vital role in exploring the evolution of binary stars (H.-L. Chen et al. 2021; T. M. Tauris & E. P. J. van den Heuvel 2023), the structure of accretion disks (C. O. Heinke et al. 2013), and the behavior of accreting millisecond pulsars, especially the development of spider pulsars (Z. L. Yang et al. 2023). To date, approximately 20 sources in our Galaxy have been confidently confirmed as UCXBs based on precise orbital period measurements (M. Armas Padilla et al. 2023). In most confirmed UCXBs, NSs act as the accretor. The source X9 in the globular cluster 47 Tucanae was thought to be a possible BH UCXB candidate, whose nature remains undetermined (A. Bahramian et al. 2017; P. Charles 2017; M. Armas Padilla et al. 2023).

UCXBs in the Galactic field are believed to result from binary star evolution through four channels: (i) a white dwarf (WD) transferring matter through the Roche-lobe overflow (RLOF) to an NS/BH (J. E. Pringle & R. F. Webbink 1975; L. R. Yungelson et al. 2002; Z. Wang & D. Chakrabarty 2004; R. Sengar et al. 2017), (ii) a helium (He) star donor providing He-rich material to fill its Roche lobe (G. J. Savonije et al. 1986; L. R. Yungelson 2008; B. Wang et al. 2021), (iii) a low-mass main-sequence (MS) star near the end of hydrogen core burning filling its Roche lobe with initial orbital periods shorter than the bifurcation period (L. A. Nelson et al. 1986; P. Podsiadlowski et al. 2002; M. V. van der Sluys et al. 2005; S. Yu et al. 2021), and (iv) the accretion-induced collapse of ONe WDs in binaries (T. M. Tauris et al. 2013; B. Wang & D. Liu 2020; D. Liu & B. Wang 2023). These evolutionary scenarios highlight the profound role of UCXBs in studying accretion physics, angular momentum loss, and the interplay between gravitational and nuclear processes (C. O. Heinke et al. 2013; H.-L. Chen et al. 2021; T. M. Tauris & E. P. J. van den Heuvel 2023). Beyond their relevance to compact binary systems, UCXBs also offer broader insights into astrophysics, providing a window into stellar evolution under extreme conditions (C. O. Heinke et al. 2013).

The advent of gravitational-wave (GW) astronomy has revolutionized our understanding of the Universe, with space-based observatories poised to open a new frontier in low-frequency GW detection (P. Amaro-Seoane et al. 2017). UCXBs, with their short orbital periods, are key targets for space-based GW detectors such as LISA (P. Amaro-Seoane et al. 2023), Tianqin (J. Luo et al. 2016), and Taiji (W.-H. Ruan et al. 2020). During their inspiraling phases, UCXBs emit low-frequency GW signals, providing crucial insights into binary interactions, envelope ejection, and compact binary evolution (G. Nelemans et al. 2000; N. Ivanova et al. 2013). Studying UCXBs through these observatories not only enhances our understanding of these systems but also enriches the broader field of astrophysics by revealing the fundamental physics governing their behavior (C. O. Heinke et al. 2013; P. Amaro-Seoane et al. 2023).

However, the GW radiation from UCXBs, combined with the low-mass MS companion channel, is not well studied. We focus on this channel in the current study, where UCXBs originate from low-mass MS stars near the end of hydrogen

core burning. This channel, despite its potential significance, has been underexplored compared to other formation pathways. we simulate the evolutionary pathways of potential UCXBs from zero-age MS (ZAMS) stars and model their corresponding GW signals. The simulated companion stars in our study have notably low masses, aligning well with previous works in the field (W.-C. Chen et al. 2020). By comparing the simulated signals with the detection capabilities of space-based GW observatories and incorporating observational data from confirmed UCXB sources, this study validates the feasibility of detecting UCXBs through GW astronomy and underscores their importance as astrophysical laboratories for extreme conditions.

2. GW Radiation from UCXBs

UCXBs are characterized by their very short orbital periods, typically less than 1 hr, and involve complex mass transfer processes during their evolution. Due to their tight orbits and high mass densities, UCXBs are significant sources of GWs (G. Nelemans & P. G. Jonker 2010; W.-C. Chen et al. 2020).

2.1. GW Emission Characteristics in UCXBs

The characteristics of GW emission in these systems can be understood through the frequency, strain amplitude, and radiation power.

For a circular binary system, the GW frequency depends on the orbital period. It can be expressed as

$$f_{\rm gw} = \frac{2}{P_{\rm orb}}. \tag{1}$$

By analyzing the frequency, we can further deduce the corresponding strain. The strain amplitude can be expressed as

$$h_0 = \frac{2(GM_c)^{5/3}}{c^4}\left(\frac{\pi f_{\rm gw}}{D}\right)^{2/3}, \tag{2}$$

where $M_c = \frac{(m_1 m_2)^{3/5}}{(m_1+m_2)^{1/5}}$ is the chirp mass and D is the distance to the source.

The radiation power $P_{\rm gw}$ emitted by UCXBs due to GWs, which significantly impact the orbital period, mass transfer rate, and energy (G. Nelemans & P. G. Jonker 2010), is given by

$$P_{\rm gw} = \frac{32}{5}\frac{(2\pi)^{8/3}}{G^{5/3}c^5}\frac{(m_1 m_2)^2}{(m_1+m_2)^{1/3}P_{\rm orb}^{10/3}}. \tag{3}$$

These relationships highlight how the orbital dynamics of UCXBs drive GW emission, with shorter orbital periods producing higher-frequency and higher-amplitude signals.

2.2. Mass Transfer

In UCXBs, mass transfer occurs through RLOF. As the donor star fills its Roche lobe, material is transferred to the compact object through an accretion disk (L. M. van Haaften et al. 2012). The mass transfer rate ($\dot{M}_d$) is determined by the formula

$$\dot{M} = \frac{2\dot{J}}{J\left(\frac{\Delta R_1}{\Delta m_1} - \frac{\Delta R_2}{\Delta m_2}\right)}, \tag{4}$$

where J is the orbital angular momentum and $\frac{\Delta R_1}{\Delta M_1}$, $\frac{\Delta R_2}{\Delta M_2}$ describe the sensitivity of the donor and Roche-lobe radii to mass changes, respectively.

Initially, the shrinking orbit driven by GW radiation causes a rapid increase in the mass transfer rate. The orbital evolution of UCXB systems under the influence of GW radiation during the mass transfer process exhibits significant complexity. In general, GW radiation acts to reduce the orbital separation by extracting angular momentum from the system. However, in certain cases, if the mass transfer rate is sufficiently high, the system's total angular momentum may increase, leading to an increase in orbital separation (G. Nelemans et al. 2001; K. A. Postnov & L. R. Yungelson 2014; Y. Guo et al. 2022). This expansion, in turn, may lead to a reduction in the mass transfer rate and a potential decrease in the efficiency of GW radiation emission.

2.3. Energy Loss and Orbital Decay

The energy carried away by GWs leads to orbital decay. This continuous energy loss through GW radiation is a critical factor in the orbital decay process (L. M. van Haaften et al. 2012). The rate of energy loss due to gravitational radiation is given by

$$\frac{dE}{dt} = -\frac{32}{5}\frac{G^4}{c^5}\frac{(m_1 m_2)^2(m_1+m_2)}{a^5}, \tag{5}$$

where a is the orbital separation. As the separation decreases, the rate of energy loss increases, leading to faster orbital decay. The corresponding rate of orbital period change is given by

$$\frac{dP_{\rm orb}}{dt} = -\frac{96\pi G^{5/3}}{5c^5}\left(\frac{2\pi}{P_{\rm orb}}\right)^{5/3}\frac{m_1 m_2}{(m_1+m_2)^{1/3}}. \tag{6}$$

These equations demonstrate the close interplay between energy loss and orbital evolution, which ultimately leads to mergers that produce compact remnants such as NSs or BHs (B. Wang et al. 2021).

2.4. Detector Capability

UCXBs emit GWs within the sensitivity range of space-based GW observatories such as Taiji, TianQin, and LISA. These observatories are designed to detect low-frequency GWs.

The detectability of GW signals can be quantified by the signal-to-noise ratio (SNR),

$$\mathrm{SNR} = \sqrt{4\int_0^\infty \frac{|\tilde{h}(f)|^2}{S_n(f)}\,df}, \tag{7}$$

where $\tilde{h}(f)$ is the Fourier transform of the GW signal and $S_n(f)$ is the noise spectral density of the detector. Observations over longer durations enhance the SNR as

$$\mathrm{SNR} \propto \sqrt{T}. \tag{8}$$

Taiji and LISA, both optimized for low-frequency GWs, excel in detecting the early inspiral phases of UCXBs, while TianQin's geocentric orbit enhances its sensitivity to systems nearing merger. Together, these observatories provide complementary insights into the full evolutionary pathway of UCXBs, covering both early inspiral and late merger stages.

Typically, an SNR greater than 5 or 8 is considered to indicate a credible detection.

The above formulae and parameters will serve as the foundation for our model to simulate the evolution of UCXBs and their GWs, allowing us to better evaluate the capability of space-based GW detectors to detect GWs from UCXBs.

3. Population Synthesis and GW Simulation Model

3.1. Population Synthesis Model

To reliably simulate the GW radiation of UCXBs, we employ the Compact Object Mergers: Population Astrophysics and Statistics (COMPAS) code (J. Riley et al. 2022). This tool is specifically designed to model the evolution of compact object binaries, starting from the ZAMS and progressing through critical stages, including supernova kick, mass transfer, common envelope (CE) evolution, RLOF, and the formation of compact objects.

A key feature of COMPAS is its ability to rapidly estimate the evolution of binary systems using approximate models, which allows for the exploration of large parameter spaces. This approach, while computationally efficient, may limit the detailed physical accuracy of certain stages, such as the CE and RLOF phases, which involve complex and highly nonlinear processes.

The CE phase plays a crucial role in the evolution of UCXBs, where the primary star expands and engulfs its companion, forming a shared gas envelope. This phase induces a significant loss of angular momentum, driving the binary components closer together. In COMPAS, angular momentum loss mechanisms such as magnetic braking and GW radiation are incorporated using parameterized models (P. C. Peters 1964). The energy balance in the CE phase is described by the $\alpha_{\rm CE}$ formalism, which simplifies the process but captures its overall effects on binary evolution.

RLOF is another key phase in UCXBs' evolution, during which mass transfer occurs as the donor star fills its Roche lobe. The Roche-lobe radius (R_L) is approximated by the following relation (U. Kolb & H. Ritter 1990):

$$\frac{R_L}{a} \approx \frac{0.49q^{2/3}}{0.6q^{2/3} + \ln(1 + q^{1/3})}, \tag{9}$$

where a is the orbital separation and q is the mass ratio of the binary system, defined as $q = \frac{m_2}{m_1}$.

Building on its success in modeling the binaries BH–BH, BH–NS, and NS–NS (T. Wagg et al. 2022b), COMPAS is extended here to simulate the formation and evolution of UCXBs. Using large-scale binary population synthesis, we estimate the population properties of UCXBs to evaluate their detectability by space-based GW detectors. This approach highlights the statistical trends of UCXBs rather than their detailed evolution, providing a comprehensive framework for understanding their role as GW sources.

In this context, we employed the COMPAS binary evolution code to simulate a comprehensive parameter space, to investigate the formation and evolution of UCXBs. The grid spans the following ranges: the initial accretor mass (M_1) ranges from 6 to 12 $M_\odot$ with a step size of 0.1 $M_\odot$, and the initial donor star mass (M_2) spans 0.4–1.2 $M_\odot$ with a step size of 0.01 $M_\odot$. The initial orbital radius (R) ranges from 0.5 to 10 au in increments of 0.5 au, and the system metallicity is varied between 0.001 and 0.01 with a step size of 0.001. This parameter grid ensures a thorough exploration of UCXBs' potential formation pathways and evolutionary outcomes. All simulations assume circular orbits, consistent with the low eccentricity typically observed in UCXBs due to tidal forces.

Starting from a ZAMS binary system in the COMPAS code, the evolution to a UCXB involves several key stages. Initially, the system consists of two close binary stars on the MS, with a significant mass difference between them (e.g., $M_1/M_2 > 8$). The more massive primary star evolves into a red giant, losing mass through stellar winds. Despite this mass loss, the core of the primary may undergo a supernova explosion, leading to the formation of a compact object, such as an NS or BH. Meanwhile, the donor star remains on the MS and undergoes mass transfer to the compact object, typically through RLOF, resulting in significant angular momentum loss. This process may trigger CE evolution, and the CE phase is often unstable, leading to additional mass loss and further orbital contraction. The orbital period decreases, eventually forming an LMXB. As the orbit becomes extremely tight, the efficiency of mass transfer from the donor to the compact object increases, leading to the formation of a UCXB from the MS companion channel. According to the model proposed by J. Riley et al. (2022), a star is assumed to experience an electron-capture supernova if its He core mass falls within the range of 1.6–2.25 $M_\odot$, while stars with He core masses exceeding 2.25 $M_\odot$ are expected to undergo core-collapse supernovae. These formation criteria are crucial for understanding the subsequent evolution of UCXBs.

3.2. GW Simulation Model

To simulate the GW signals of UCXBs, we employ the LISA Evolution and Gravitational Wave Orbit Kit (LEGWORK; T. Wagg et al. 2022a). This Python-based toolkit enables simulations of orbital dynamics, GW signal prediction, and detector sensitivity. LEGWORK natively supports the LISA and Tianqin detectors (T. Robson et al. 2019), and we adapt it to the Taiji model by replacing the sensitivity parameters of LISA with those specific to Taiji (W.-H. Ruan et al. 2020).

The sensitivity of the Taiji detector can be described by the following equation, similar to that of LISA, which accounts for noise contributions from the optical metrology system, single-test mass acceleration, and galactic confusion noise:

$$S_n(f) = \frac{1}{L^2}\left(P_{\rm OMS}(f) + 2\left(1 + \cos^2\left(\frac{f}{f_*}\right)\right)\frac{P_{\rm acc}(f)}{(2\pi f)^4}\right) \times \frac{1}{R} + S_c(f), \tag{10}$$

where L is the detector arm length, $f_* = \frac{c}{2\pi L}$ is the transfer frequency, $P_{\rm OMS}(f)$ is the optical metrology noise, $P_{\rm acc}(f)$ is the single-test mass acceleration noise, and $S_c(f)$ is the galactic confusion noise.

For the response function R, we adopted an approximate estimation to simplify the calculations while maintaining sufficient accuracy. The response function describes the detector's sensitivity to GW signals at different frequencies, and its approximate form is given by

$$R = \frac{3}{10}\left(1 + 0.6\left(\frac{f}{f_*}\right)^2\right). \tag{11}$$

Using the parameters, we implement the Taiji sensitivity curve into LEGWORK and compare it with the LISA sensitivity curve. As shown in Figure 1, Taiji demonstrates

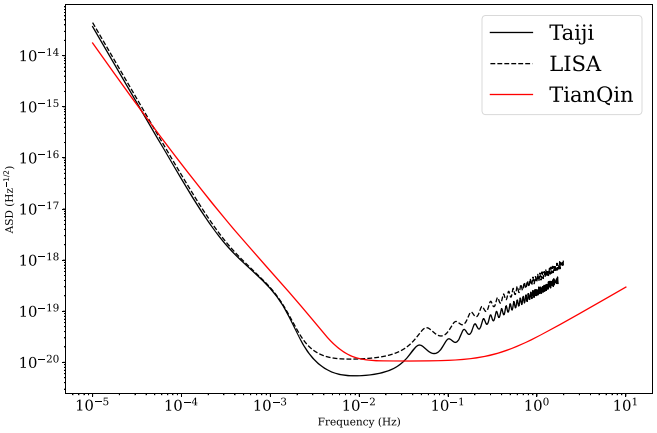

Figure 1. The figure presents the sensitivity curves of the Taiji, LISA, and TianQin detectors. The solid black line represents the sensitivity of the Taiji detector, the dashed line represents the sensitivity of the LISA detector, and the red line represents the sensitivity of the TianQin detector. All curves are plotted as ASD vs. frequency.

improved sensitivity in specific frequency ranges compared to LISA, particularly at lower frequencies, making it better suited for detecting inspiral stages of UCXBs.

The Tianqin sensitivity curve is also implemented in LEGWORK, enabling a comparison of its performance against Taiji and LISA. Tianqin is optimized for higher-frequency signals, with its sensitivity curve given by

$$S_n(f) = \frac{10}{3L^2}\left(\frac{4S_a}{(2\pi f)^4}\left(1+\frac{1\times 10^{-4}}{f}\right)+S_x\right) \times\left(1+0.6\left(\frac{f}{f_*}\right)^2\right)+S_c(f). \quad (12)$$

LEGWORK has been successfully applied to simulate GWs from compact object binaries, including binary BHs and NS binaries (T. Wagg et al. 2022b). In this study, we extend its application to UCXBs, focusing on modeling their GW characteristics and evaluating their detectability by comparing these signals with detector sensitivity curves.

Additionally, LEGWORK's capability to incorporate observational data provides a unique opportunity to align theoretical models with real astrophysical systems. By integrating data from confirmed UCXBs, we enhance the accuracy of simulated GW signals, ensuring that they reflect realistic astrophysical parameters. This approach not only validates the robustness of LEGWORK but also provides a framework for testing the detectability of UCXBs under varying observational scenarios. Such simulations are essential for advancing the design and optimization of future GW detection missions and deepening our understanding of UCXBs as key sources in the low-frequency GW regime.

4. Observational Data on UCXBs

The study of UCXBs began in the late 1970s with the HEAO-1 satellite (K. S. Wood et al. 1984), which pioneered the identification of X-ray properties in compact binary systems. Since then, continuous advancements in observational techniques have facilitated the discovery of UCXBs using instruments such as RXTE (K. Jahoda et al. 1996), Chandra (M. C. Weisskopf et al. 2000), XMM-Newton (F. Jansen et al. 2001), and Swift (N. Gehrels et al. 2004).

RXTE, with its advanced timing capabilities and broad energy range, played a crucial role in studying UCXBs. Notably, it facilitated the discovery of accreting millisecond X-ray pulsars such as XTE J1751–305, enabling precise mass measurements (C. B. Markwardt et al. 2002). These findings significantly advanced our understanding of compact object physics and binary evolution.

The Chandra X-ray Observatory, launched by NASA in 1999, is among the most advanced X-ray telescopes, offering unparalleled imaging and spectroscopic capabilities. Chandra has significantly contributed to the study of UCXBs by resolving fine details of X-ray emissions and structures. For instance, observations of 4U 1916–05 revealed X-ray dips that provided critical insights into the system's geometry and dynamics (A. M. Juett & D. Chakrabarty 2006). Additionally, Chandra's data on 47 Tuc X9 identified it as a potential BH UCXB, deepening our understanding of these rare systems (C. O. Heinke et al. 2005).

XMM-Newton, launched by the European Space Agency (ESA) in 1999, has significantly advanced the study of UCXBs. Its high sensitivity and spectroscopic capabilities have yielded critical data on systems such as IGR J17062–6143 (J. V. Hernández Santisteban et al. 2019) and 2S 0918–549 (F. Koliopanos et al. 2014), offering new insights into their emission mechanisms and orbital properties.

Swift has been instrumental in discovering and confirming new UCXB systems through its combined X-ray and optical observational capabilities. By detecting X-ray bursts and corresponding optical changes, Swift has established the nature of several candidates. Notably, it observed an outburst from Swift J0911.9–6452, enabling a detailed study of this source. Furthermore, Swift identified Swift J1756.9–2508 as a confirmed UCXB (H. A. Krimm et al. 2007), providing crucial insights into the nature and evolution of these compact systems.

Precise distance measurements are essential for studying GWs from UCXBs. The Gaia mission, launched by the ESA in 2013, has revolutionized astrometry by providing accurate positions, distances, and proper motions for over a billion stars. Gaia's data significantly improve the distance estimates for UCXBs such as 2S 0918–549, 4U 1543–624 (H. A. Krimm et al. 2007), and 47 Tuc X9 (S. Chen et al. 2018). In our study, we reference data from Gaia DR2, utilizing the distances of some known UCXBs to calculate and simulate GW emissions.

We acknowledge that there is significant uncertainty regarding the evolutionary channels of UCXBs; for example, XTE J1751–305 could potentially have evolved from an ONe WD + He WD system (D. Liu & B. Wang 2023). We chose five sources with a broad range of orbital periods and distances. Among the 20 known UCXBs, previous studies have investigated the formation and evolution of 15 of them in detail using multiwavelength observational data (F. Koliopanos et al. 2014; S. Prodan & N. Murray 2015; J. V. Hernández Santisteban et al. 2019; W. Yuan et al. 2025), providing some insight and potential constraints for theoretical studies on the formation and evolution of UCXBs (W.-C. Chen et al. 2020; K. Qin et al. 2023, 2024). However, for the remaining five systems, there is still considerable uncertainty and ongoing discussion regarding their possible evolutionary channels. Considering the relative contributions of different UCXB formation channels, and based on the relatively stable X-ray emission characteristics observed in these five UCXBs (P. B. Hemphill et al. 2021; R. M. Ludlam et al. 2021), this

Table 1
Information of Selected UCXBs

ID	Name	R.A.	Decl.	D (kpc)	$P_{\rm orb}$ (minutes)	M_1 ($M_\odot$)	M_2 ($M_\odot$)
1	4U 1543–624	15:47:54.69	−62:34:05.4	$3.3^{+6.5}_{-1.4}$	$18.2^{+0.1}_{-0.1}$	1.4	0.0432
2	4U 1626–67	16:32:16.79	−67:27:39.3	$3.5^{+2.3}_{-1.3}$	$41.538^{+0.002}_{-0.002}$	1.4	0.0189
3	XTE J1751–305	17:51:13.49	−30:37:23.4	8.5	$42.42235^{+0.00006}_{-0.00006}$	1.4	0.0185
4	XTE J0929–314	09:29:20.19	−31:23:03.2	10	$43.57910^{+0.00005}_{-0.00005}$	1.4	0.0181
5	4U 1916–053	19:18:47.87	−05:14:17.09	$7.6^{+0.4}_{-0.4}$	$49.75^{+0.16}_{-0.16}$	1.4	0.0158

Note. M_1 is assumed to be the mass of a standard NS (fixed at 1.4 $M_\odot$), while M_2 is estimated using the formula by W.-C. Chen et al. (2020). Distances and orbital periods of the selected UCXBs are derived from direct observational data, as reported in previous studies (J. Middleditch et al. 1981; F. M. Walter et al. 1982; D. K. Galloway et al. 2002; C. B. Markwardt et al. 2002; A. M. Juett & D. Chakrabarty 2006).

study tentatively proposes that they might be candidates for the low-mass MS companion channel in UCXB formation.

To present the observational data, Table 1 provides key observational parameters for five selected UCXBs. The listed parameters are essential for our analysis and simulations, offering insights into the physical and orbital properties of these systems. Given the influence of tidal forces, UCXBs typically exhibit near-circular orbits with very low eccentricity. Thus, the calculations presented in the table assume circular orbits ($e = 0$; G. Nelemans et al. 2000).

5. Results and Discussion

From the ZAMS, we evolved the binary systems and identified 48 potential UCXB systems. We also attempted to enlarge the samples of primordial ZAMS binaries in the COMPAS binary evolution code, but the results indicated that the simulation had already reached convergence. Therefore, variations in the initial sample size on the order of millions would not significantly impact the evolved parameters of UCXBs in our simulations. Analysis of their initial conditions reveals distinct trends across parameters, including accretor and donor star masses, orbital radii, and metallicity distributions, as illustrated in Figure 2.

The accretor mass (M_1) distribution is centered around 9.5 $M_\odot$, with most systems falling between 8 $M_\odot$ and 11 $M_\odot$, suggesting that moderately massive accretors are more conducive to UCXB formation. Donor star masses (M_2) exhibit a broad distribution, with prominent clustering around 0.7 $M_\odot$ and 1.0 $M_\odot$, reflecting a wide range of viable mass transfer rates that contribute to the diversity of UCXBs. The initial orbital separations (R) are predominantly concentrated between 4 and 6 au, highlighting the importance of moderate separations for UCXB formation. Excessively wide orbits fail to initiate efficient mass transfer, while overly tight orbits risk premature mergers. This distribution underscores the delicate balance required between orbital separation and stellar evolutionary timescales. The metallicity distribution skews toward lower values, with most systems around 0.002. Low-metallicity environments favor UCXB formation by reducing stellar wind mass loss, enabling binaries to retain more mass. This stabilizes mass transfer and enhances the likelihood of binaries shrinking into the ultracompact phase.

Following the evolution of the systems, we analyzed the final parameters of the UCXBs. These systems exhibited significant changes in their accretor and donor masses, orbital radius, and periods. By examining the evolved conditions of the UCXBs, we observed several key trends, as shown in Figure 3.

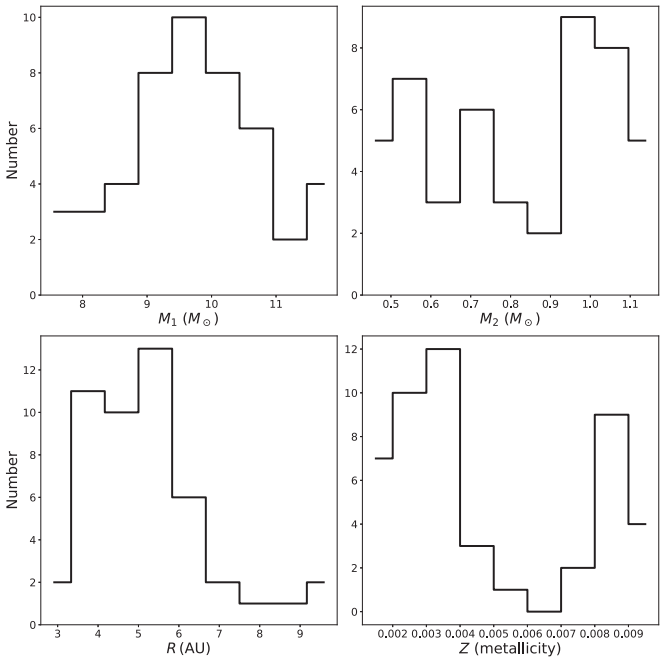

Figure 2. Distributions of the initial conditions for the simulated UCXB systems. The panels show the distributions of M_1, M_2, R, and metallicity.

The figure illustrates the distributions of evolved parameters for simulated UCXB systems, highlighting the final stages of their evolution in terms of M_1, M_2, R, and orbital period. These distributions provide insight into the characteristics of UCXBs as they evolve into their ultracompact phase.

For the M_1 distribution, most evolved accretor masses lie between 1.6 $M_\odot$ and 2.3 $M_\odot$. The dashed line at 2.1 $M_\odot$ marks the threshold used to distinguish NSs from possible BHs. Systems with accretor masses exceeding 2.1 $M_\odot$ are likely candidates for BH UCXBs, indicating that some systems may evolve into BHs rather than NSs. This distinction underscores the diversity of outcomes in the evolutionary pathways of UCXBs.

The M_2 distribution shows that the majority of donor stars have masses below 0.1 $M_\odot$, consistent with significant mass loss over time. Such low masses reflect advanced stages of donor evolution, where prolonged mass transfer has nearly depleted the donor star, leaving it with minimal mass. This feature is characteristic of UCXBs nearing the ultracompact phase. Previous research has shown that the ultracompact phase resulting from the NS + MS companion evolutionary channel

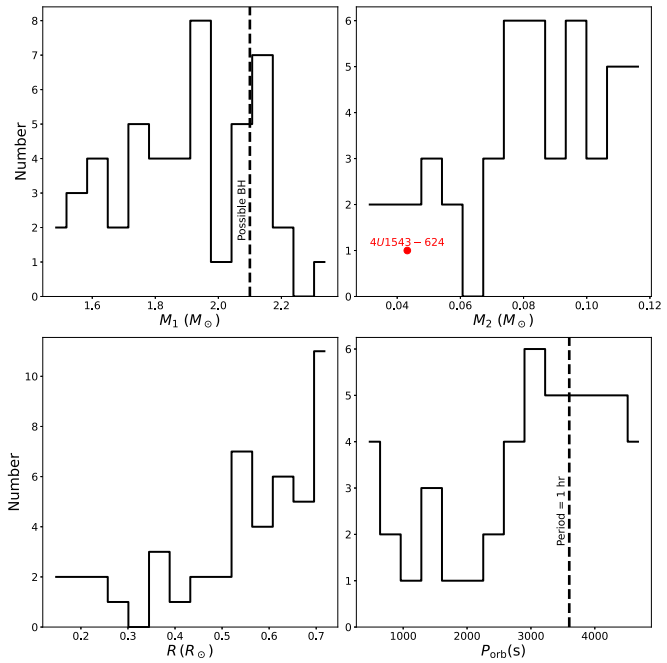

Figure 3. Distributions of the evolved parameters for the simulated UCXB systems, showing M_1, M_2, R, and orbital period. The dashed lines indicate the assumed possible BH and critical orbital period of 1 hr.

begins with a companion star mass around 0.1 $M_\odot$ (W.-C. Chen et al. 2020).

The third panel shows the distribution of orbital radius (R), where most systems have compact orbits, ranging from 0.5 $R_\odot$ to 0.7 $R_\odot$. These tight radii are driven by continuous mass transfer and GW radiation, which gradually shrink the orbits. Such compact orbits are a defining trait of UCXBs, facilitating the conditions for sustained mass transfer and orbital tightening.

In the orbital period distribution, most systems exhibit periods under 1 hr, which is typical for UCXBs. The dashed line at 1 hr indicates the threshold for confirmed UCXBs, though we extend the classification to systems with periods up to 90 minutes to encompass more potential UCXB candidates. Some extreme cases show periods as short as 10 minutes, illustrating advanced stages of orbital contraction due to GW radiation. These distributions capture the wide range of evolutionary paths observed in UCXBs, validating the model's ability to reflect the diversity of UCXB systems found in nature.

5.1. The Evolution of UCXBs

In this section, we explore the detailed orbital evolution of UCXB systems, focusing on the results generated using the LEGWORK tool. The simulation results, as illustrated in Figure 4, demonstrate a gradual increase in the orbital frequency over time, driven primarily by GW radiation. This steady increase reflects the stable shrinking of the binary's orbit as it evolves toward the ultracompact phase.

The later stages of evolution show a sharp rise in orbital frequency, underscoring the accelerating effect of GW emission on orbital tightening. This rapid contraction phase marks a critical period where the binary emits intense GW signals, making it particularly significant for observational studies.

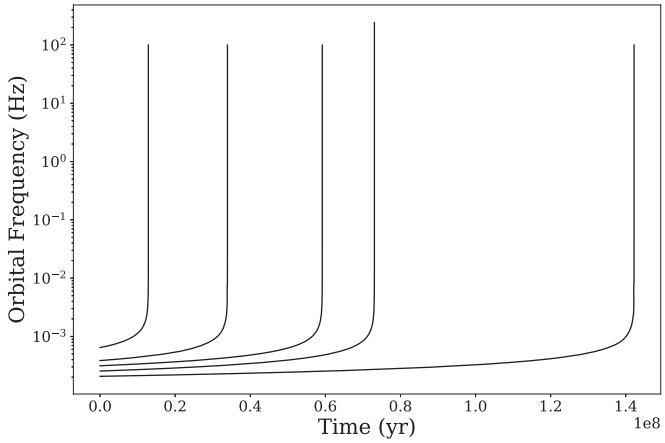

Figure 4. Orbital frequency evolution of the UCXB system, generated using LEGWORK.

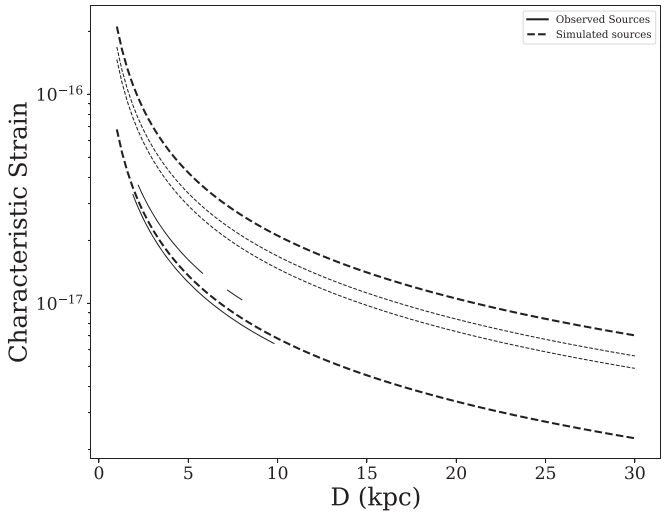

Figure 5. Characteristic strain as a function of distance for observed and simulated UCXB sources. The solid lines represent observed sources, while the dashed lines show simulated sources.

From our simulations, the lifetimes of UCXBs formed through the MS channel are approximately 50–150 Myr, defined as the period during which the systems emit detectable GW signals. This result is consistent with Wang et al. (B. Wang et al. 2021), who reported similar lifetimes for UCXBs from the MS channel. These systems evolve more gradually due to their lower initial mass transfer rates, allowing for a longer detection window and sustained GW emission. Despite rapid changes near the end of their lifetimes, the systems remain dynamically stable for the majority of their evolution, ensuring that UCXBs are long-lived sources of GWs. This stability and prolonged GW emission make UCXBs particularly valuable targets for space-based GW detectors, which can track their signals across different evolutionary stages, providing insights into their dynamics and the underlying physics of compact binaries.

5.2. Simulated GW Characteristics of UCXBs

5.2.1. Properties of the GWs

Using the LEGWORK package, we calculated the characteristic strain for 48 simulated UCXB systems. In Figure 5, we plot the upper and lower bounds of the characteristic strain

as a function of distance, covering the range from 1 to 30 kpc. This plot illustrates how the characteristic strain systematically decreases as the distance from the source increases, providing a clear depiction of the expected GW emissions from UCXBs. The dashed lines in the figure represent the upper and lower bounds of the characteristic strain for the simulated UCXBs, which gives a comprehensive view of the emission profile for different systems.

Additionally, we utilized the data from Table 1 to calculate the chirp mass and characteristic strain for the selected UCXBs and then overlaid these calculated characteristic strains onto the simulated data. The solid lines represent these observed sources, and the range of characteristic strains accounts for uncertainties in their measured distances (Gaia Collaboration et al. 2016). By plotting these observed systems alongside the simulated ones, we can directly compare their characteristic strains. This comparison highlights the alignment between real observations and our simulation results.

The fact that the observed sources fall within the range of characteristic strains predicted by our simulations confirms that the model may capture the key physical processes underlying UCXB evolution and GW emission, making it a reliable tool for predicting the GW characteristics and validating its application for future studies. This reinforces the notion that UCXBs are stable and detectable sources of GWs, in terms of both their long-term evolution and their GW emissions across a range of distances.

5.2.2. The Sensitivity Curve and the Population of Sources

In this study, we conducted GW signal simulations for simulated UCXBs as well as observed UCXBs, which are likely formed through the MS channel, using the LEGWORK tool to analyze these systems. Our simulated UCXB sources distributed randomly within a distance range of 2–12 kpc, reflecting realistic observational uncertainties and typical distances of known UCXBs.

We then evaluated their detectability with the space-based GW detectors Taiji and TianQin. Our research focuses on the performance of the detectors over different observation periods (short-term: 1 yr; medium-term: 4 yr; and long-term: 8 yr) and analyzes their potential to detect UCXBs, particularly in terms of frequency and SNR.

The amplitude spectral density (ASD) is a measure of the noise in a GW detector as a function of frequency. It is derived from the noise power spectral density (PSD), $S_n(f)$, where f is the frequency. The ASD is defined as the square root of the PSD:

$$\mathrm{ASD}(f) = \sqrt{S_n(f)}\ [\mathrm{Hz}^{-1/2}]. \tag{13}$$

The ASD provides a convenient way to visualize the sensitivity of a detector across different frequency bands. A lower ASD value corresponds to a more sensitive detector at a given frequency. In GW astronomy, the ASD is commonly used to compare the sensitivity of detectors.

We compared the performance of Taiji and TianQin in detecting UCXBs across different frequency bands and identified their respective advantages and limitations. Taiji exhibits superior detectability in the low-frequency range (approximately 10^{-4}–10^{-2} Hz), while TianQin's strength lies in the high-frequency range (approximately 10^{-2}–1 Hz). However, considering the frequency distribution of UCXBs, they are primarily concentrated in Taiji's optimal detection range (10^{-4}–10^{-2} Hz), which makes Taiji more favorable for UCXB detection overall.

By comparing the simulated UCXBs systems with observed UCXBs, we validated the reliability of the simulations. Our results indicate that only systems with SNR > 5 are likely to be detected reliably. Although prior studies such as those of W.-C. Chen et al. (2020) provided valuable insight into detectability by focusing on the characteristic strain exceeding the detector sensitivity curve, this approach establishes an upper limit for the detection reliability of GW signals. By incorporating SNR into our analysis using LEGWORK, we improve the evaluation of detectable sources and emphasize the importance of extended observation durations in improving both sensitivity and detection confidence.

The simulated GW signals are in good agreement with the observed UCXBs, demonstrating that our models may predict UCXBs that future space-based detectors could observe.

As illustrated in Figure 6, LISA and Taiji show remarkable sensitivity in the low-frequency range, making them capable of detecting more low-frequency UCXBs. Over longer observation periods, their ability to detect weaker and more distant sources improves significantly. This detection confirms LISA and Taiji's observational capabilities, particularly in identifying UCXBs in the low-frequency range, and underscores the reliability of its performance over extended observation periods. TianQin is also capable of detecting simulated UCXBs and can successfully capture these sources over extended observation periods. These results highlight the critical role of extended observation times in improving the sensitivity of space-based detectors and their ability to capture a greater number of simulated UCXB sources, thereby deepening our understanding of their GW signals. Thus, TianQin's contributions to joint observations are vital for constructing a more comprehensive picture of the UCXB population and improving the overall understanding of their GW emissions.

Figure 7 illustrates the detectability of UCXB systems by Taiji, showing the distribution of sources across orbital periods and their corresponding SNRs. The heat map highlights that most simulated sources fall within Taiji's sensitivity range, particularly for systems with shorter orbital periods (below 30 minutes) and higher SNRs. The gradual increase in source counts as SNR rises reflects Taiji's strong ability to detect a substantial portion of the UCXB population, particularly in the low-frequency regime where these systems predominantly reside.

The red dots represent observed UCXBs, and the error bars associated with these points originate from uncertainties in distance measurements (Gaia Collaboration et al. 2016). These uncertainties directly affect the derived SNR, as the SNR depends on the inverse square of the distance to the source. Despite these uncertainties, the alignment of observed UCXBs with the simulated source distribution demonstrates the reliability of the models in capturing the characteristics of UCXBs. Taiji's ability to encompass these systems within its sensitivity range underscores its potential as a highly capable instrument for studying UCXBs and their GW emissions.

Figure 8 illustrates the detectability of UCXB systems by TianQin. The heat map shows that TianQin generally achieves lower SNRs compared to Taiji but achieves its highest sensitivity for UCXBs with extremely short orbital periods. These systems are located in the high-frequency range where

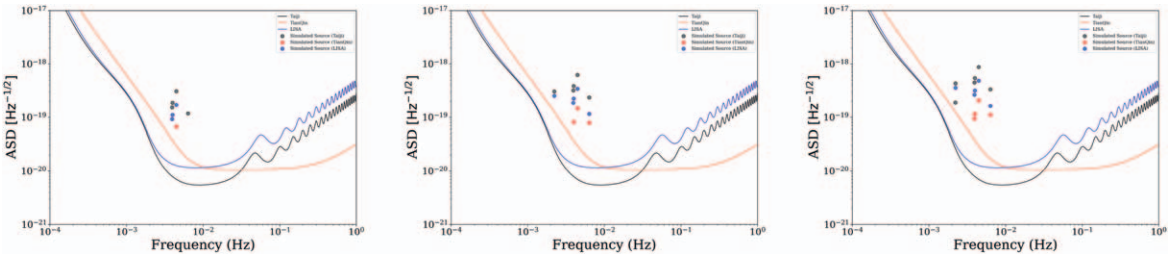

Figure 6. ASD as a function of frequency for both simulated and observed UCXB systems, overlaid with the sensitivity curves of Taji (black line) and TianQin (red line). From left to right, the panels depict results for observation periods of 1 yr, 4 yr, and 8 yr. The circles represent simulated UCXB sources.

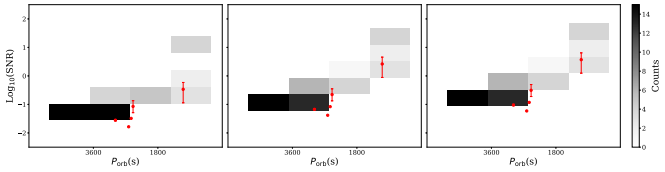

Figure 7. Distribution of SNR in logarithmic scale ($\log_{10}(\mathrm{SNR})$) as a function of orbital period by Taiji. The gray-scale shading indicates the count of sources in each bin, with darker shades representing higher counts. Red points represent real UCXBs, and error bars indicate the uncertainty in their measurements. Panels from left to right correspond to observation periods of 1 yr, 4 yr, and 8 yr.

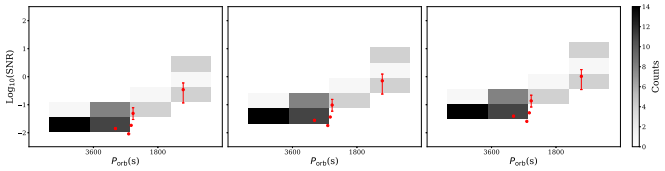

Figure 8. Similar to Figure 7, we present the distribution of SNR in logarithmic scale ($\log_{10}(\mathrm{SNR})$) as a function of orbital period for TianQin.

TianQin excels, making it especially suitable for detecting such compact and fast-evolving sources.

By combining the observations from LISA, Taiji, and TianQin, the joint data provide a significantly more reliable and robust approach to detecting UCXBs. Each detector has its own unique noise characteristics and sensitivity profiles, and cross-referencing data from different instruments greatly improves the precision of the detections. This synergy not only enhances the overall reliability of our findings but also ensures that UCXBs are identified with higher accuracy and confidence.

More importantly, joint observations enable the precise localization of UCXBs by exploiting the timing differences in the signals received by the detectors. Given that LISA, Taiji, and TianQin are positioned at different locations in space and are sensitive to distinct portions of the frequency spectrum, combining their data allows for the triangulation of the source's position with much greater certainty. This cross-checking across detectors and frequency ranges helps to refine the sky map, reducing the uncertainty in source localization.

By leveraging the complementary strengths of the detectors, joint observations not only enhance detection accuracy but also play a pivotal role in improving the precision of UCXB localization. This refined localization ensures that sources are pinpointed with greater confidence, even when their signals are faint or distant.

We roughly calculated the combined SNR for joint observations using the following formula:

$$\mathrm{SNR}_{\mathrm{combined}} = \sqrt{\mathrm{SNR}_1^2 + \mathrm{SNR}_2^2}. \tag{14}$$

This equation assumes that the noise contributions of each detector are uncorrelated, providing a straightforward way to calculate the enhancement in SNR through joint observations. The results demonstrate significant improvements in detection confidence when combining data from multiple detectors, as summarized in Table 2.

Besides the increase in the observable number of simulated UCXBs, we emphasize that the well-known source 4U 1543–624 achieves a combined SNR greater than 5 under long-term observations by Taiji and LISA. This result strongly supports the importance of joint observations, highlighting their significance for studying actual UCXBs.

5.3. Estimating the Current Observable Population of UCXBs from the Low-mass MS Companion Channel

To estimate the current observable number of UCXBs from the MS companion channel in the Milky Way, we focused on binary systems satisfying specific initial conditions: $M_1 = 8$–$12\,M_\odot$, $M_2 = 0.5$–$1.2\,M_\odot$, $R = 3$–9 au, and $Z = 0.002$–0.01, as shown in Figure 2. Note that in our simulations, we assumed that these stars form simultaneously, which is a simplifying assumption for this study. From our simulations, this parameter space contained 339,669 binaries, within which 48 UCXBs formed, yielding a formation rate of

$$P_{\mathrm{UCXB\text{-}Simulated}} = \frac{48}{339,669} \approx 1.41 \times 10^{-4}. \tag{15}$$

The total number of binaries in the Milky Way is estimated as (T. C. Licquia & J. A. Newman 2015)

$$N_{\mathrm{binary}} = (5 \times 10^{10} \text{ to } 2.4 \times 10^{11}). \tag{16}$$

The initial mass function follows the Kroupa form (P. Kroupa 2001; G. Chabrier 2003):

$$\xi(M) \propto M^{-\alpha}, \quad \alpha = \begin{cases} 1.3, & \text{if } M < 0.5\,M_\odot, \\ 2.3, & \text{if } M > 0.5\,M_\odot. \end{cases} \tag{17}$$

The combined fraction f_{Initial} is the product of mass fraction f_{mass}, orbital radius fraction f_R (G. Duchêne & A. Kraus 2013), and metallicity fraction f_Z. These fractions are calculated as follows:

$$f_{\mathrm{mass}} \approx 0.004, \quad f_R \approx 0.12, \quad f_Z \approx 0.20, \tag{18}$$

Table 2
Counts of Simulated UCXBs Detected (SNR > 5) for Detectors and Their Combinations

Observation Time	TianQin	LISA	Taiji	LISA + TianQin	Taiji + TianQin	Taiji + LISA	All Detectors
1 yr	1	3	4	4	4	4	4
4 yr	3	5	5	5	5	6	6
8 yr	4	5	6	6	6	7	7

so the total initial fraction is

$$f_{\rm Initial} = f_{\rm mass} \times f_R \times f_Z = 0.004 \times 0.12 \times 0.20 = 0.000096. \quad (19)$$

The total number of UCXBs from the MS companion channel formed over Galactic history is

$$N_{\rm total} = f_{\rm Initial} \times N_{\rm binary} \times P_{\rm UCXB\text{-}Simulated} = (676\text{–}3243). \quad (20)$$

A typical UCXB from this channel has a lifetime of 100 Myr (B. Wang et al. 2021) and a Galactic star formation history of 10 Gyr. We assume that UCXBs are formed uniformly over time, meaning the formation rate of UCXBs is constant at all time points throughout the evolution of the Milky Way. Based on this, the fraction currently observable is

$$\frac{\text{lifetime}}{\text{Galactic star formation duration}} = 0.01. \quad (21)$$

Thus, the current observable number is

$$N_{\rm current} = N_{\rm total} \times 0.01 = (7\text{–}32). \quad (22)$$

In summary, our simulations suggest that the Milky Way currently hosts approximately 7–32 observable UCXBs from the MS companion channel, depending on the total binary population and initial parameter distributions. This range is broadly consistent with the five selected UCXBs that have been observed to date. The agreement between our theoretical predictions and the observed sample strengthens the reliability of the simulations and validates the parameter space selected for the formation of UCXBs from the MS companion channel.

6. Conclusion

This study provides a comprehensive analysis of UCXB formation and evolution using the COMPAS binary evolution code, starting from the ZAMS. While the COMPAS code relies on certain approximations and simplifications, which means the study may not capture all aspects of UCXB evolution in a fully comprehensive manner, it still generates results that are consistent with the known properties of UCXBs. By modeling the entire evolutionary history of UCXBs, rather than focusing solely on specific stages of RLOF or CE phases, we explore a broader range of evolution. Although the study is not exhaustive, it provides a solid foundation for understanding UCXB evolution and produces results that align well with the observed characteristics of UCXBs.

Our study also advances the detectability analysis of UCXBs as GW sources by incorporating SNR calculations into population synthesis models. Although previous studies, such as those by W.-C. Chen et al. (2020), relied mainly on characteristic strain comparisons to detector sensitivity curves, our approach evaluates the detection reliability more realistically. We specifically compute SNR values for different observation durations and apply a threshold of SNR > 5 to provide a robust framework for assessing the detectability of UCXBs, particularly for observations with LISA, Taiji, and TianQin. The alignment of our simulated GW signals with the ASD curves of these detectors validates the feasibility of detecting UCXBs formed through MS donor channels, even at distances up to 12 kpc. These results may indicate the robustness of our simulations and could potentially highlight the importance of extended observation durations in improving the detection of distant and marginal sources.

In addition, our analysis estimates that the Milky Way currently hosts approximately 7–32 observable UCXBs from the MS companion channel. This range is broadly consistent with the observed data so far, suggesting that our simulations and selected parameter space may reflect the real population of UCXBs from the MS companion channel in the Galaxy. The agreement between theoretical predictions and observational data not only strengthens the validity of our modeling framework but also highlights the potential of space-based GW observatories to identify more UCXBs in the future.

Based on our simulations, Taiji or LISA alone could detect one to six UCXBs from the MS companion channel in the Milky Way over a long-term observation period, while TianQin could detect one to four sources. Joint observations with TianQin and LISA could enhance this number, improve localization, and contribute to a deeper understanding of UCXBs as GW sources. This underscores the importance of both individual and collaborative observations for uncovering the galactic population of these UCXBs.

Furthermore, due to the significant influence of mass on GW signals, we argue that space-based GW detectors such as Taiji and LISA are well suited to capturing BH UCXBs. The inclusion of BH UCXBs as potential sources expands the scope of GW astronomy, highlighting the capability of these detectors to explore both classical and less-studied compact binary populations.

Our findings confirm that UCXBs, particularly those with extreme orbital periods, are significant sources of GWs within the sensitivity ranges of next-generation space-based detectors. The combination of stable GW emission over long timescales and intense signals during late-stage orbital contraction underscores their importance as key targets for future observations. By employing population synthesis, we provide a detailed and realistic view of UCXB formation and evolution, emphasizing the importance of modeling the entire evolutionary path rather than focusing on individual phases. This approach enables the identification of new UCXB formation pathways and contributes to a deeper understanding of their role in the broader context of compact binary evolution.

In conclusion, this work significantly strengthens the case for UCXBs as important sources in multimessenger astronomy. By providing a comprehensive framework for their formation, evolution, and detectability, it lays the groundwork for future observational missions and theoretical studies.

Acknowledgments

This work was supported by the Tianshan Talent Training Program through the grant 2023TSYCCX0101, the Central Guidance for Local Science and Technology Development Fund under No. ZYYD2025QY27, the National Natural Science Foundation of China NSFC 12433007, and the science research grants from the China Manned Space Project with No. CMS-CSST-2021-A08.

ORCID iDs

Jinzhong Liu https://orcid.org/0000-0002-7420-6744

References

Amaro-Seoane, P., Andrews, J., Arca Sedda, M., et al. 2023, LRR, 26, 2
Amaro-Seoane, P., Audley, H., Babak, S., et al. 2017, arXiv:1702.00786
Armas Padilla, M., Corral-Santana, J. M., Borghese, A., et al. 2023, A&A, 677, A186
Bahramian, A., Heinke, C. O., Tudor, V., et al. 2017, MNRAS, 467, 2199
Chabrier, G. 2003, PASP, 115, 763
Charles, P. 2017, AAS/High Energy Astrophysics Division, 16, 108.17
Chen, H.-L., Tauris, T. M., Han, Z., & Chen, X. 2021, MNRAS, 503, 3540
Chen, S., Richer, H., Caiazzo, I., & Heyl, J. 2018, ApJ, 867, 132
Chen, W.-C., Liu, D.-D., & Wang, B. 2020, ApJL, 900, L8
Duchêne, G., & Kraus, A. 2013, ARA&A, 51, 269
Gaia Collaboration, Prusti, T., de Bruijne, J. H. J., et al. 2016, A&A, 595, A1
Galloway, D. K., Chakrabarty, D., Morgan, E. H., & Remillard, R. A. 2002, ApJL, 576, L137
Gehrels, N., Chincarini, G., Giommi, P., et al. 2004, ApJ, 611, 1005
Guo, Y., Wang, B., & Han, Z. 2022, MNRAS, 515, 2725
Heinke, C. O., Grindlay, J. E., Edmonds, P. D., et al. 2005, ApJ, 625, 796
Heinke, C. O., Ivanova, N., Engel, M. C., et al. 2013, ApJ, 768, 184
Hemphill, P. B., Schulz, N. S., Marshall, H. L., & Chakrabarty, D. 2021, ApJ, 920, 142
Hernández Santisteban, J. V., Cúneo, V., Degenaar, N., et al. 2019, MNRAS, 488, 4596
Ivanova, N., Justham, S., Chen, X., et al. 2013, A&ARv, 21, 59
Jahoda, K., Swank, J. H., Giles, A. B., et al. 1996, Proc. SPIE, 2808, 59
Jansen, F., Lumb, D., Altieri, B., et al. 2001, A&A, 365, L1
Juett, A. M., & Chakrabarty, D. 2006, ApJ, 646, 493
Kolb, U., & Ritter, H. 1990, A&A, 236, 385
Koliopanos, F., Gilfanov, M., Bildsten, L., & Trigo, M. D. 2014, MNRAS, 442, 2817
Krimm, H. A., Markwardt, C. B., Deloye, C. J., et al. 2007, ApJL, 668, L147
Kroupa, P. 2001, MNRAS, 322, 231
Licquia, T. C., & Newman, J. A. 2015, ApJ, 806, 96
Liu, D., & Wang, B. 2023, MNRAS, 521, 6053
Ludlam, R. M., Jaodand, A. D., García, J. A., et al. 2021, ApJ, 911, 123
Luo, J., Chen, L.-S., Duan, H.-Z., et al. 2016, CQGra, 33, 035010
Markwardt, C. B., Swank, J. H., Strohmayer, T. E., in 't Zand, J. J. M., & Marshall, F. E. 2002, ApJL, 575, L21
Middleditch, J., Mason, K. O., Nelson, J. E., & White, N. E. 1981, ApJ, 244, 1001
Nelemans, G., & Jonker, P. G. 2010, NewAR, 54, 87
Nelemans, G., Verbunt, F., Yungelson, L. R., & Portegies Zwart, S. F. 2000, A&A, 360, 1011
Nelemans, G., Yungelson, L. R., & Portegies Zwart, S. F. 2001, A&A, 375, 890
Nelson, L. A., Rappaport, S. A., & Joss, P. C. 1986, ApJ, 304, 231
Peters, P. C. 1964, PhRv, 136, 1224
Podsiadlowski, P., Rappaport, S., & Pfahl, E. D. 2002, ApJ, 565, 1107
Postnov, K. A., & Yungelson, L. R. 2014, LRR, 17, 3
Pringle, J. E., & Webbink, R. F. 1975, MNRAS, 172, 493
Prodan, S., & Murray, N. 2015, ApJ, 798, 117
Qin, K., Jiang, L., & Chen, W.-C. 2023, ApJ, 944, 83
Qin, K., Xu, K., Liu, D.-D., et al. 2024, ApJ, 961, 110
Rappaport, S., Joss, P. C., & Webbink, R. F. 1982, ApJ, 254, 616
Riley, J., Agrawal, P., Barrett, J. W., et al. 2022, ApJS, 258, 34
Robson, T., Cornish, N. J., & Liu, C. 2019, CQGra, 36, 105011
Ruan, W.-H., Guo, Z.-K., Cai, R.-G., & Zhang, Y.-Z. 2020, IJMPA, 35, 2050075
Savonije, G. J., de Kool, M., & van den Heuvel, E. P. J. 1986, A&A, 155, 51
Sengar, R., Tauris, T. M., Langer, N., & Istrate, A. G. 2017, MNRAS, 470, L6
Tauris, T. M., Sanyal, D., Yoon, S. C., & Langer, N. 2013, A&A, 558, A39
Tauris, T. M., & van den Heuvel, E. P. J. 2023, Physics of Binary Star Evolution. From Stars to X-ray Binaries and Gravitational Wave Sources (Princeton, NJ: Princeton Univ. Press)
van der Sluys, M. V., Verbunt, F., & Pols, O. R. 2005, A&A, 431, 647
van Haaften, L. M., Nelemans, G., Voss, R., Wood, M. A., & Kuijpers, J. 2012, A&A, 537, A104
Wagg, T., Breivik, K., & de Mink, S. E. 2022a, ApJS, 260, 52
Wagg, T., Broekgaarden, F. S., de Mink, S. E., et al. 2022b, ApJ, 937, 118
Walter, F. M., Mason, K. O., Clarke, J. T., et al. 1982, ApJL, 253, L67
Wang, B., Chen, W.-C., Liu, D.-D., et al. 2021, MNRAS, 506, 4654
Wang, B., & Liu, D. 2020, RAA, 20, 135
Wang, Z., & Chakrabarty, D. 2004, ApJL, 616, L139
Weisskopf, M. C., Tananbaum, H. D., Van Speybroeck, L. P., & O'Dell, S. L. 2000, Proc. SPIE, 4012, 2
Wood, K. S., Meekins, J. F., Yentis, D. J., et al. 1984, ApJS, 56, 507
Yang, Z. L., Han, J. L., Jing, W. C., & Su, W. Q. 2023, ApJL, 956, L39
Yu, S., Lu, Y., & Jeffery, C. S. 2021, MNRAS, 503, 2776
Yuan, W., Dai, L., Feng, H., et al. 2025, SCPMA, 68, 239501
Yungelson, L. R. 2008, AstL, 34, 620
Yungelson, L. R., Nelemans, G., & van den Heuvel, E. P. J. 2002, A&A, 388, 546